

The Temperature Effect on Sensitivity of Direct Detection Optical Receiver Incorporating FET- Amplifier

Abdulgaffar S. M.

Elect.and electronic Eng. Dept.
College of Engineering
Thi-Qar University

RafidM.Hannun

Elect.and electronic Eng. Dept.
College of Engineering
Thi-Qar University
eng_rafid005@yahoo.com

Muhannad Sahib Ali

Mech. Eng. Dept.
College of Engineering
Thi-Qar University

Abstract

It is known that temperature rise boosts the generations of electron-holes pairs in semiconductors and increases their conductivity that obtained to increase noise. High Electron Mobility Transistors (HEMTs) gives many advantages like low noise and high associated gain at microwave frequencies. Different shapes and places in containers are done to analyze the temperature effect on chips with other thermal and aerodynamic parameters.

In this paper, the performance of integrated optical receiver consisting of PIN (Positive Intrinsic Negative)-photodiode and HEMT-based transimpedance type amplifier is analyzed upon the effect of temperature variation. Variation of temperature occurs when change device space in one block covers. The simulation results show that the sensitivity (P_{sen}) of an optical receiver is minimal in space when temperature effect is low if it is based on well-designed HEMT.

المستخلص

تؤدي ارتفاع درجات الحرارة في اشباه الموصلات الى توليد أزواج إلكترون فجوة التي تؤدي الى زيادة الموصلية والتي تزيد من الضجيج. الترانزسترات ذات حركة الإلكترونات العالية عدة ميزات كانخفاض الضجيج والرياح المصاحب العالي في ترددات الموجات الدقيقة المايكروية. تم اختيار مواقع وأشكال مختلفة للحيز الذي يحتوي هذه الدقائق الإلكترونية لتحليل تأثير درجة الحرارة عليها ودراسة بعض الخصائص الحرارية والايروديناميكية لها.

تم في هذا البحث تحليل اداء المستلم البصري المتكامل المتكون من داوود ضوئي نوع PIN الممانعة الانتقالية المعتمدة على HEMT, تم هذا التحليل بالاعتماد على تأثير تغير درجة الحرارة. ان تغير درجة الحرارة يحدث عند تغيير شكل وفضاء الحيز الذي يحتوي هذه الاجهزة. نتائج المحاكاة بينت ان الحساسية للمستلم البصري تكون الاقل في الفضاء الذي يكون فيه تغير درجة الحرارة قليل عندما يكون تصميم HEMT جيد.

1. Introduction

The continuing minimization of electronic devices has significantly contributed to rapid developments in electronic technology. Miniaturization is, however, characterized by high heat dissipation per unit area of electronic components. Therefore, an effective cooling strategy is required to avoid premature failure and to ensure enhanced reliability and life expectancy of electronic components. Despite various cooling techniques and recent developments in the electronic industry, air cooling is still considered to be not only a cheap and readily available option but also a very effective technique.

The optoelectronic device that recovers the transmitted electrical signal from the incident light wave signal is optical receiver. It is formed from a photo detector (photodiode), connected to a FET-based amplifier. It is represented by PIN photodiode. Theoretical sensitivities for both PIN/FET direct-detection receivers are shown in Figure(1)[1, 2].

HEMTs based on AlGaAs/InGaAs structure given many advantages due to their low noise [3], and high associated gain at microwave frequencies [1]. Therefore, they are well suited to the preamplifier requirements of broadband light wave receivers.

It is expected that the monolithic integration of optical and electronic components on the same chip will alternatively lead to ultra-high speed, high sensitivity, reliability, and low cost [4,5]. Most of wide band optical receivers have been fabricated by integrating a PIN photodiode for light detection [3], and a transimpedance amplifier for electronic signal amplification and impedance matching [6].

In this paper the performance(sensitivity) is analyzed for a monolithically integration optical receiver consisting of a PIN photodiode and an FET-based transimpedance type preamplifier through variation of temperature to determine the optimum space with minimum effect of temperature.

The resulting boundary layer equations for a two-dimensional vertical flow, with variable fluid (air) properties except density, for which the Boussinesq approximations are used, are then written as [7, 8]:

$$\frac{\partial u}{\partial x} + \frac{\partial v}{\partial y} = 0 \quad (1)$$

$$u \frac{\partial u}{\partial x} + v \frac{\partial v}{\partial y} = g\beta(T - T_{\infty}) + \frac{1}{\rho} \frac{\partial}{\partial y} \left(\mu \frac{\partial u}{\partial y} \right) \quad (2)$$

$$\rho c_p \left[\frac{\partial u}{\partial x} + \frac{\partial v}{\partial y} \right] = \frac{\partial}{\partial y} \left(k \frac{\partial T}{\partial y} \right) + q''' + \beta T u \frac{\partial P_a}{\partial x} \mu \left(\frac{\partial u}{\partial y} \right)^2 \quad (3)$$

where the last two terms in the energy equation are the dominant terms from pressurework and viscous dissipation effects. Here u and v are the velocity components in the x and y directions, respectively. Although these equations are written for a vertical, two-dimensional flow, similar approximations can be employed for many other flow circumstances, such as axisymmetric flow over a vertical cylinder and the wake above a concentrated heat source.

2. Receiver

2.1 Description

In this paper, the optical receiver is considered to consist of an InGaAs PIN photodiode integrated with a single gain stage trans impedance amplifier as shown in Fig (1). The design of preamplifier provides (i) a wide bandwidth; and (ii) high dynamic range, which is defined as the range of input power levels over which the bit error rate is acceptable [9]. All of the loads in the circuit are active to allow for integration with the other HEMTs and to reduce device area and overall power dissipation of the circuit. A feedback convention resistor is replaced by a transistor (Q_3) with an equivalent output resistance R_F . The FET feedback can be used to reduce parasitic shunt capacitance, thereby resulting in a wide bandwidth operation.

2.2 Receiver noise sources

The receiver current noise consists of thermal noise in the feedback resistor, FET channel noise, low frequency (LF) noise and shot noise due to the leakage in the FET gate and the detector. Contributions noise in an optical receiver are determined by [5, 9]:

$$\sigma_{sh} = \sqrt{2q(I_{Dark} + I_{leak})I_2 B} \quad (4)$$

$$\sigma_{ch} = 4\pi C_T B \sqrt{\frac{kT\Gamma I_3 B}{g_m}} \quad (5)$$

$$\sigma_{LF} = 4\pi C_T B \sqrt{\frac{2kT\Gamma f_c I_f}{g_m}} \quad (6)$$

$$\sigma_{th} = 2 \sqrt{\frac{kT I_2 B}{R_F}} \quad (7)$$

Here, σ_{sh} , σ_{ch} , σ_{LF} , and σ_{th} are the shot noise, channel noise, LF noise, and thermal noise respectively, g_m is the extrinsic transconductance, T is the temperature, k is the Boltzmann constant, B is the data bit-rate, I_{Dark} is the PIN dark current, q is the electronic charge, I_{leak} is the gate leakage current, Γ is the HEMT noise figure (≈ 1.6 [5]), f_c is the LF corner frequency, and C_T is the total front-end capacitance. C_T is determined by:

$$C_T = C_{st} + C_{PD} + C_{GS} \quad (8)$$

where, C_{st} is the input stray capacitance, C_{PD} is the PIN diode capacitance, and C_{GS} is the HEMT gate-source capacitance. I_f , I_2 , and I_3 are effective receiver bandwidth integrals which depend on the transfer function of the circuit and the input and output waveforms. A NRZ data format is assumed, and a raised cosine output pulse response of the receiver for a rectangular pulse shape.

2.3 Receiver sensitivity

The sensitivity of receiver is given in terms of minimum, time-averaged incident optical power (P_{sen}), which can be detected for a given acceptable Bit Error Rate (BER). Assuming Gaussian noise statistics, the sensitivity is determined by [9]:

$$P_{sen} = \left(\frac{Qhf}{\eta q} \right) \sigma_T \quad (9)$$

where, η is the overall efficiency in converting the incident optical power into a signal current, h is Planck constant, f is the frequency of the incident light, $Q=6$ for $BER=10^{-9}$, and σ_T is the total noise standard deviation which is defined as:

$$\sigma_T = \sqrt{\sigma_{sh}^2 + \sigma_{ch}^2 + \sigma_{LF}^2 + \sigma_{th}^2} \quad (10)$$

Sensitivity of Receiver may be improved by decreasing the impedance at the interface. The low impedance at the PD-amplifier interface is highly non-optimal from a noise point of view, which, together with the intrinsic noise figure of the amplifier, limits receiver sensitivity.

It may be expected that the integration of monolithic transimpedance receiver is one of the facial ways to realize high sensitivity OptoElectronic Integrated Circuits (OEICs) [10].

3. Transimpedance amplifier

The PIN/transimpedance amplifier equivalent circuit is shown in Figure 2, where C_F is the stray capacitance of the feedback resistor R_F , R_{in} is the input resistance of the amplifier, A is the amplifier voltage gain, and I_{ph} is the PIN diode photocurrent.

The receiver response is represented by the transimpedance Z_T , which is the ratio of the output voltage to the input photocurrent. The frequency dependence of Z_T is calculated by [11]:

$$Z_T(f) = \frac{-AR_{in}R_F/[R_F + (I+A)R_{in}]}{1 + j \frac{2\pi f R_{in}R_F}{R_F + (I+A)R_{in}} [C_T + (I+A)C_F]} \quad (11)$$

Let Z_{T0} be the DC transimpedance, and f_{3dB} is the cutoff frequency (-3dB point), then:

$$Z_{T0} = \frac{-AR_{in}R_F}{R_F + (I+A)R_{in}} \quad (12)$$

and

$$f_{3dB} = \frac{1}{2\pi \left[\frac{R_{in}R_F}{R_F + (I+A)R_{in}} [C_T + (I+A)C_F] \right]} \quad (13)$$

Eqn. 13 is useful in determining the bandwidth of the system.

The bandwidth of the preamplifier should be at least equal to the effective noise bandwidth of the receiver (I_2B). To accomplish this, R_F must be adjusted such that f_{3dB} is equal to the effective bandwidth. Let $A \gg 1$ and $AR_{in} \gg R_F$, Eqn. 13 becomes:

$$f_{3dB} = [2\pi R_F (C_F + C_T/A)]^{-1} \quad (14)$$

then

$$R_F = [2\pi I_2 B (C_F + C_T/A)]^{-1} \quad (15)$$

Figures (3, 4) display the variation of thermal and shot of receivers noise sources as a function of bite rate, they give much prediction of receiver behavior.

Figure(6) displays the variation of sensitivity as function of bite rate.

Figures (7, 8, 9, 10) and (11, 12, 13, 14) display the variation of different receivers noise sources as a function of T. Otherwise, the parameter values used in the simulation are listed in Table(1). It is clear that the thermal and shot noises increase in the absence of temperature. At B=10 Gbit/s, the thermal noise rise is more important than that of the shot noise. The channel and LF noise behave in asame manner. However, at the same bit-rate, the channel noise and LF noise increase by factors of 1.4 and 2.08, respectively. The total noise current decreases to 0.107 of its value at 10 Gbit/s bit-rate. In Figure(6),the total noise is plotted as a function of bit-rate.

In Figure (5) R_F that satisfies the condition of negligible intersympole interference is plotted as a function of the bit-rate. Note that $R_F \approx 600 \Omega$ is required for B=10 Gbit/s. The dependence of receiver sensitivity on bit-rate is depicted in Figure(7). Note that P_{sen} (in dBs) decreases linearly with the temperature.

4. Theoretical analysis of aerodynamic and thermal parameters[13]

The heat sources simulate the components of electrical devices generating a natural convection flow in the enclosure. In addition, an externally sourced uniform air stream with a specific temperature enters the enclosure from a section located at the bottom of the enclosure (entry section) and exhausts from the upper rear section (exist section). This airflow generates a forced convection flow in the enclosure.

The equations (1, 2, 3) can be solved for domain which use air as fluid with natural convection at using the enclosure without velocity input or output and using mixed convection with using velocity input at bottom of enclosure to exit from outlet at the upper

vent. Energy equation demonstrated by equation (3) can be derived to get Prantle number of 0.7 for this type of flow. This analysis applied by the following boundary conditions:

$$u=v=0, \frac{\partial T}{\partial n}=0 \quad \text{at all the walls} \quad (16)$$

$$u=u_{in}, v=0, T=T_{atm} \quad \text{at } x=0 \text{ and } 0 \leq y \leq 5\text{cm} \quad (17)$$

$$u=u_{out}, v=0 \quad \text{at } x=x_{max} \text{ and } 25\text{cm} \leq y \leq y_{max} \quad (18)$$

$$x=x_{chip}, y=y_{chip}, q = \text{constant} \quad (19)$$

at this paper $x_{max}=60\text{cm}$ and $y_{max}=30\text{cm}$

5. Numerical analysis

To solve the equations of continuity, momentum and energy for temperature distribution domain start by the following steps:

- 1- By using GAMBIT code [12], the systems are drawn to be more than 18000 nodes depending the number of electronic devices for two dimensional space.
- 2- FLUENT 6.3 code[12] used to solve the case study by using finite volume method (one of computational fluid dynamics techniques) [8].

Steady, viscous, laminar and compressible air flow is used. The density calculated as Boussinesqequation [7]. The operating pressure is 101325 Pascal at reference location of $x=0$, $y=0$ (left bottom corner of system). The operating temperature is 300K. The heat flux rate is 10W/m^2 for any electronic device.

SIMPLE method used to solve pressure-velocity coupling with standard discretization of pressure, first order upwind discretization of momentum equation and energy equation [14].

The convergence of equations is 1×10^{-3} for continuity and velocity equations. It is 1×10^{-6} for energy.

6. Results and discussion

6-1 Sensitivity

To calculate the performance of the optical receiver, a HEMT with parameter values given in Table 1 are assumed. Other parameters used in this analysis are listed in Table 2. The HEMT performance such as g_m , C_{GS} , and C_{GD} are determined from expressions derived in Eq.(9). The HEMT capacitance and trans conductance are functions of structure parameters of the device. Therefore, it is expected that the sensitivity of HEMT-based receivers vary with transistor structure parameters.

However, the simulation results reveal that this fact loses its importance when

C_{GS} is kept much lower than $(C_{PD}+C_{st})$; or

The total front-end capacitance to trans conductance ratio (C_T/g_m) is small. In other words, the operation speed of the HEMT is much greater than the bit-rate.

Using the parameters listed in Tables (1) and(2), the PIN/HEMT optical receiver sensitivity is display in Tables(3) and(4) as a function of temperature and plotted in Figure(8) and Figure(13) as a function of T for different block form (the lower temperature induced at the design of one chip only or for three chips as shown in figure 21 to be 300.5 K). The results in this figures indicate clearly that the receiver sensitivity is less affected by the variation of T when T is small and this effect is more pronounced optimum space of receiver. For the receiver under consideration,. The simulation results indicate that P_{sen} is almost independent of the variation of T parameters. In fact, P_{sen} is minimum where T is minimum and because that the optimum space for the first block is (1) and for the second block is (2).

Figures (8, 13) present directly depend the sensitivity and temperature, also the Figures (9-12), (14- 17) offer directly dependence of the noise source with different temperature in each block.

6-2 Thermal Parameters

Eight cases of enclosure of chip design are studied at this paper. These cases are done by changing the site of chip for a typical design as shown in Figures (19, 20) and (23); case A is general for three chips, but in B the upper right chip. The lower right chip in C and the upper left chip in D. The lower mid chip is for shape (E) and the upper mid chip for F. There are two cases for half circle shape; the first is at the lower and the other isat upper. The

temperature for the first five square cases are indicated in Table (3) and for half circle in Table (4).

Figure (19) shows the velocity vectors and contours for different shapes of instrument container. For squared figure, in slide shape A it is observed that high velocity values happens at the exit (0.25 m/s) because of decreasing the density of air as a result to increasing the temperature due to the electrical and electronic devices. There is a circulation zone at the container centre. The circulation zone lies at the circumferential wall with large circle at B since one source of heat found here with low effect. Accelerated velocity at C (0.38m/s) is as a result to seven sources of heat which create strong free convection. This velocity magnitude is forced at slide contour D for low effect of obstacle to hot air passes from input vent (at low part) to output vent (at the high part). The same effect for E, but for F high velocity magnitudes takes place in comparison with all shapes to above cause. For half circle container shape, low velocity range at shape G but at H is the higher. These values are the middle values among all figures.

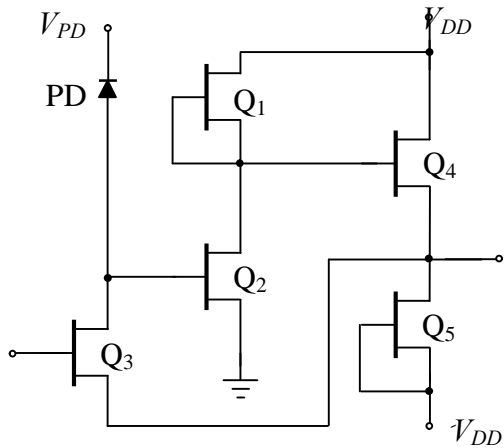
Figure (18) shows good prediction to velocity magnitude. The lower average value is near the outlet vent of system (0.52m of the horizontal dimension 0.6m) because of circulation and vortex due to the electronic devices places. But the higher is at the inlet vent. As a result to different values of velocity mentioned above and due to heat added to system because of the electronic devices, high temperature values accumulated at low velocity values. The temperature is considered as sensible heat values.

Figure (20) presented the temperature contour of domain. The range is between 300.5K to 307K for squared shape but it is between 301K to 304K for half circle shape. These differences as a result to heat added inside the system, heat rejected from the system due to free convection and the air velocity obstacle through the domain. The difference is very small as mentioned in figure. Higher temperature (307K) is at shape C and E but the lower (304K) is at shape G.

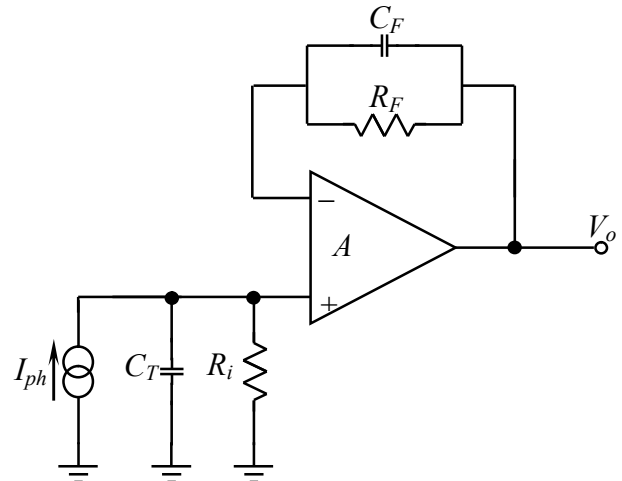
Figure (21) presented the temperature average values with horizontal axis at one domain. The highest values demonstrated here for the electronic devices places which continuously lost heat to device interior.

The pressure values in the system demonstrated by Figure (23) that give low values converged to atmospheric pressure because it is near the ground level and low temperature gradients throughout the different shapes. So, it is observed naturally low pressure values at the upper part and the higher at the low part for all shapes domain.

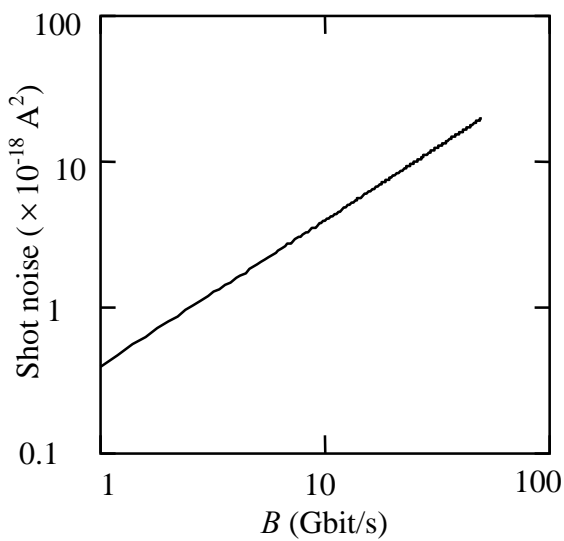
Figure (22) shows that the higher pressure value at the bottom. The average lower value is at two-third height of system.



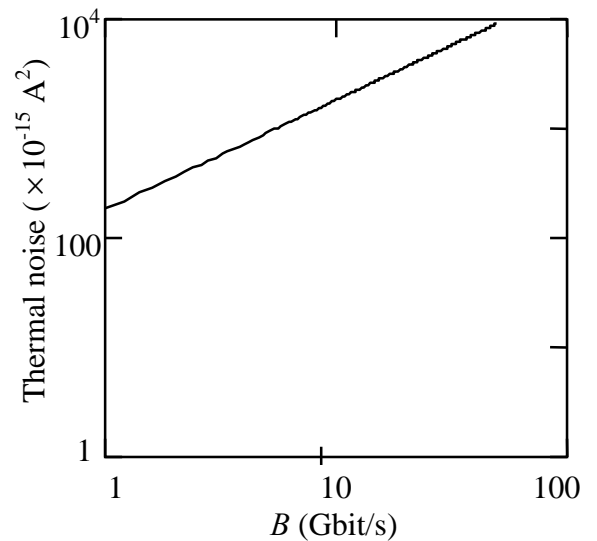
Figure(1). Circuit diagram of a transimpedance optoelectronic integrated circuit (OEIC) optical receiver.



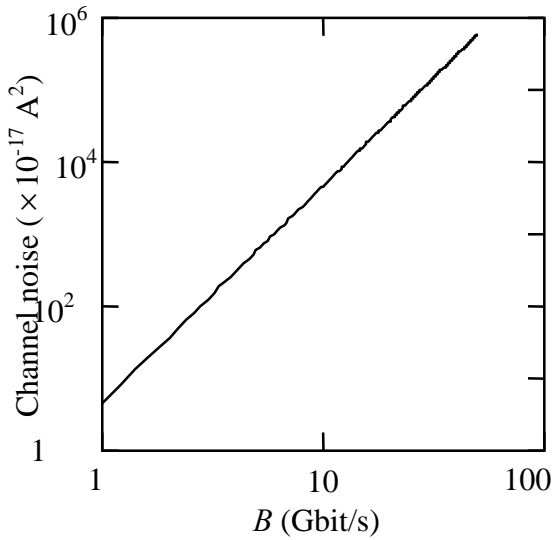
Figure(2). Equivalent circuit of the Amplifier of Figure(1).



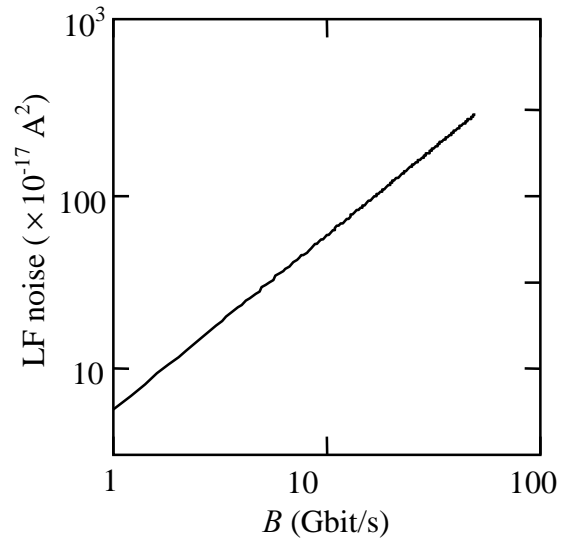
Figure(3). Variation of Shot noise as a function of B for BER of 10^{-9} .



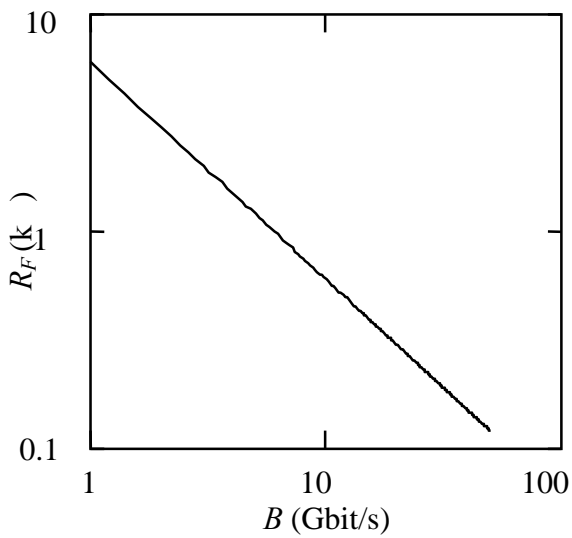
Figure(4). Variation of thermal noise as a function of B for BER of 10^{-9} .



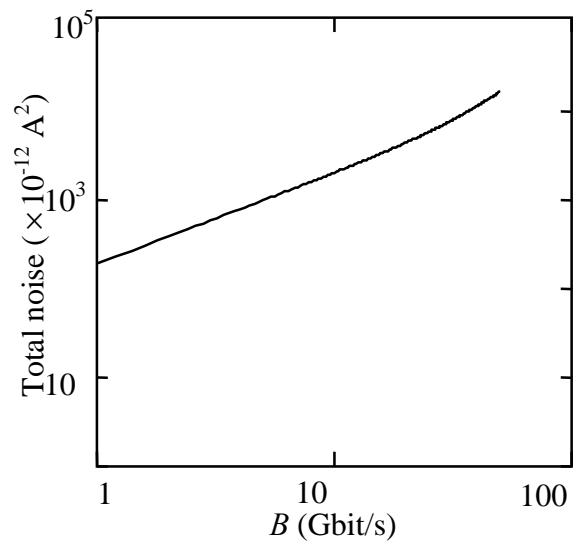
Figure(3d). Variation of Channel noise as a function of B for BER of 10^{-9} .



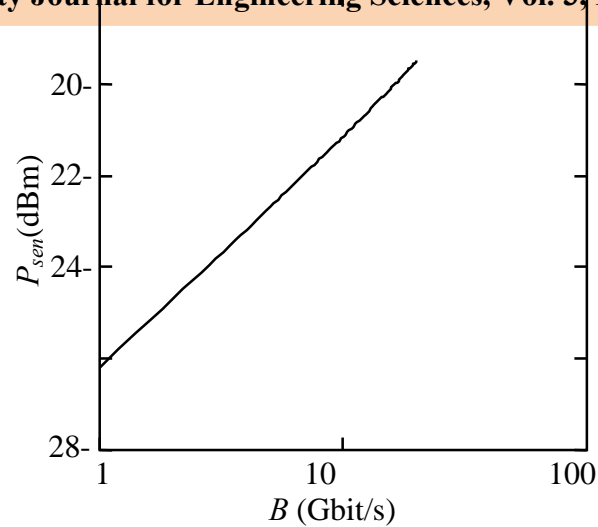
Figure(3c). Variation of LF noise as a function of B for BER of 10^{-9} .



Figure(5). Feedback resistance satisfying the condition of negligible ISI noise as a function of the bit rate.



Figure(6). Total noise as a function of bit-rate for BER of 10^{-9} .



Figure(7). Receiver sensitivity as a function of data bit-rate.

Table (1). Receiver parameters values used in the simulation.

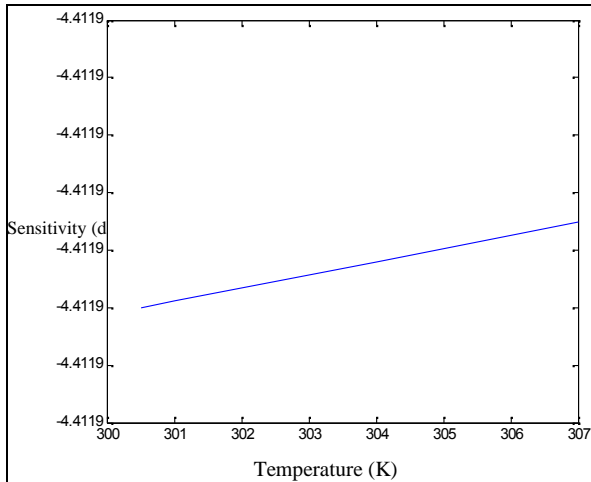
Parameter	Value	Unit
Q	6	-
I_2	0.55	-
I_3	0.085	-
I_f	0.12	-
I_{dark}	2	nA
J_{leak}	10	mA/cm ²
f_c	25	MHz
	1.55	μm
	1.6	-
	0.85	-
C_{PD}	125	fF
	-26	
C_{st}	125	fF
B	10	Gbit/s

Table (2). FET parameters used in the simulation.

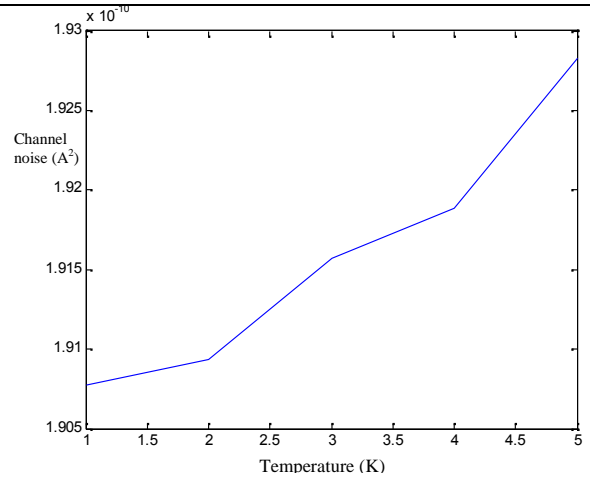
Parameter	Value	Unit
L_g	50	nm
W	50	μm
d_i	20	\AA
d_d	80	\AA
μ	12800	cm^2/Vs
v_{sat}	280×10^7	Cm/s
r	12.1	-
N_d	6×10^{18}	cm^{-3}
V_{off}	-0.017	V
R_s	1.0	
R_d	1.0	

Table (3).Sensitivity(db) as a function of temperature(K).

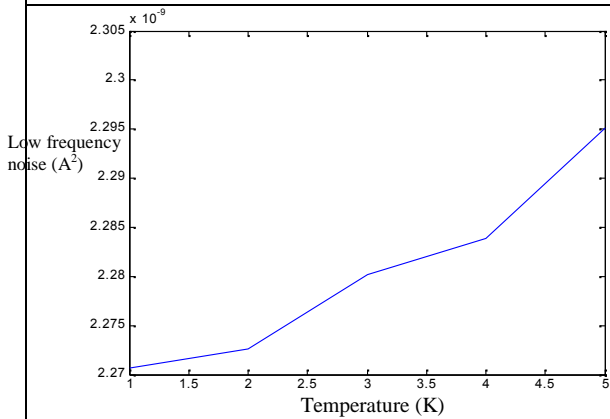
T(k)	$P_{sen}(\text{db})$
300.5	-4.41190884739970
301	-4.41190884737677
303	-4.41190884728509
304	-4.41190884723925
307	-4.41190884710172



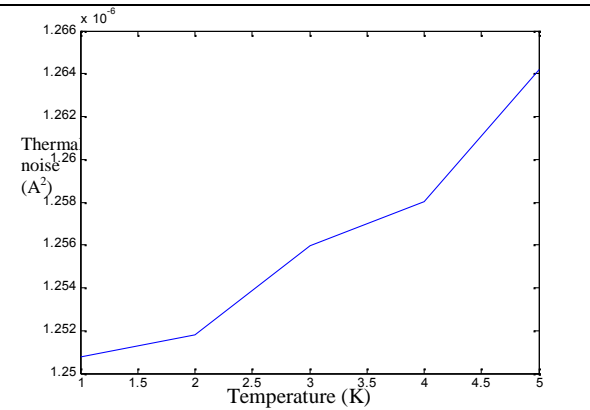
Figure(8). Sensitivity(dB) as a function of temperature(K).



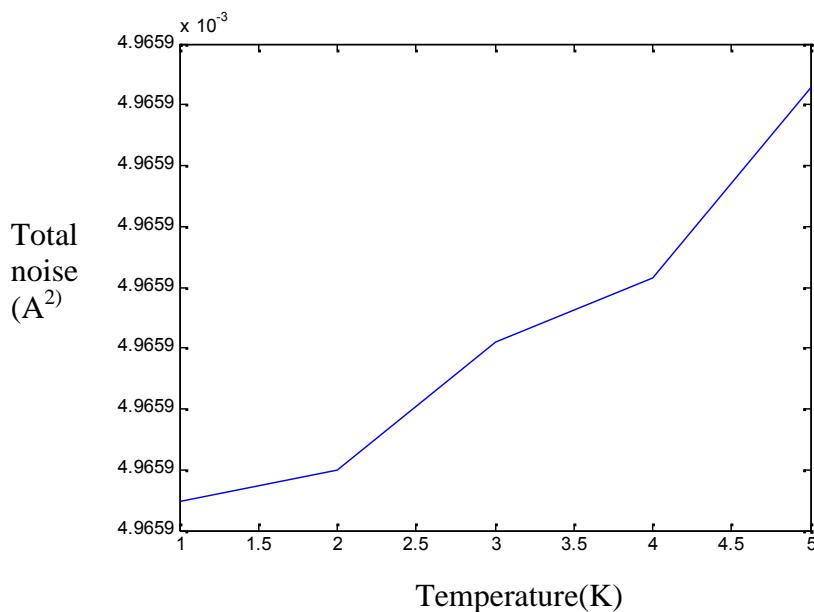
Figure(9).Low frequency noise(A²) with respect to temperature (K).



Figure(10). Channel noise(A²) as a function of temperature(K).



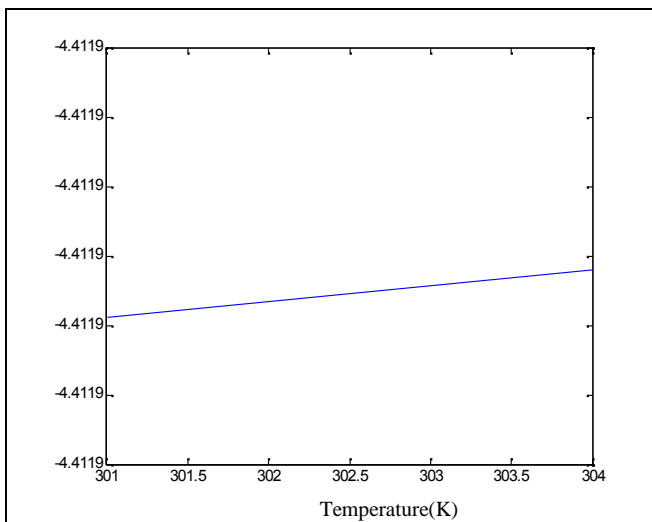
Figure(11).Thermal noise(A²) with respect to temperature(K).



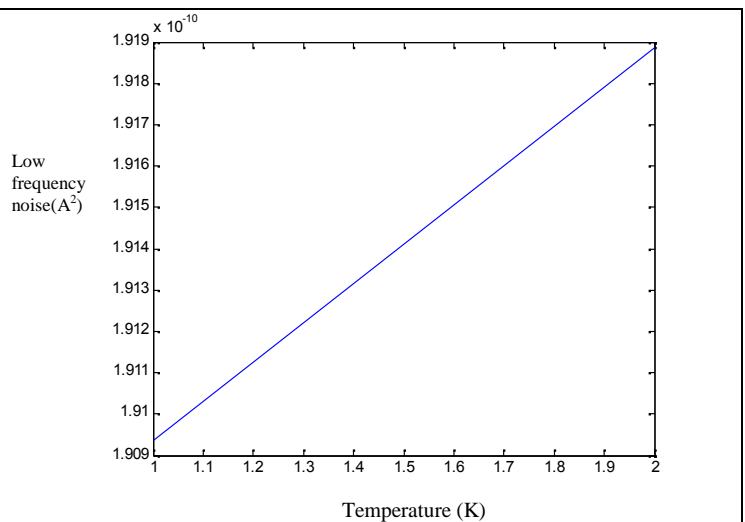
Figure(12). Total noise(A²) as a function of temperature(K) .

Table(4).Sensitivity(dB) as a function of temperature(K).

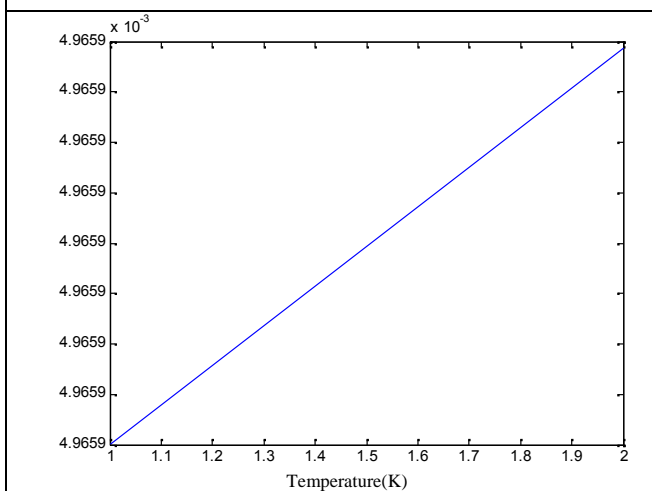
T(K)	$P_{sen}(db)$
301	-4.411908847376774
304	-4.411908847239248



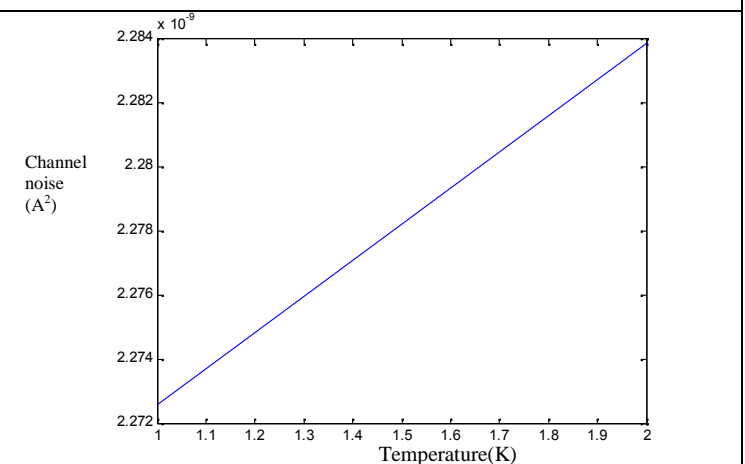
Figure(13). Sensitivity(dB) as a function of temperature(K).



Figure(14).Low frequency noise(A²) with respect to temperature(K).



Figure(15). Total noise(A²) as a function of temperature(K).



Figure(16). Channel noise(A²) with respect to temperature(K).

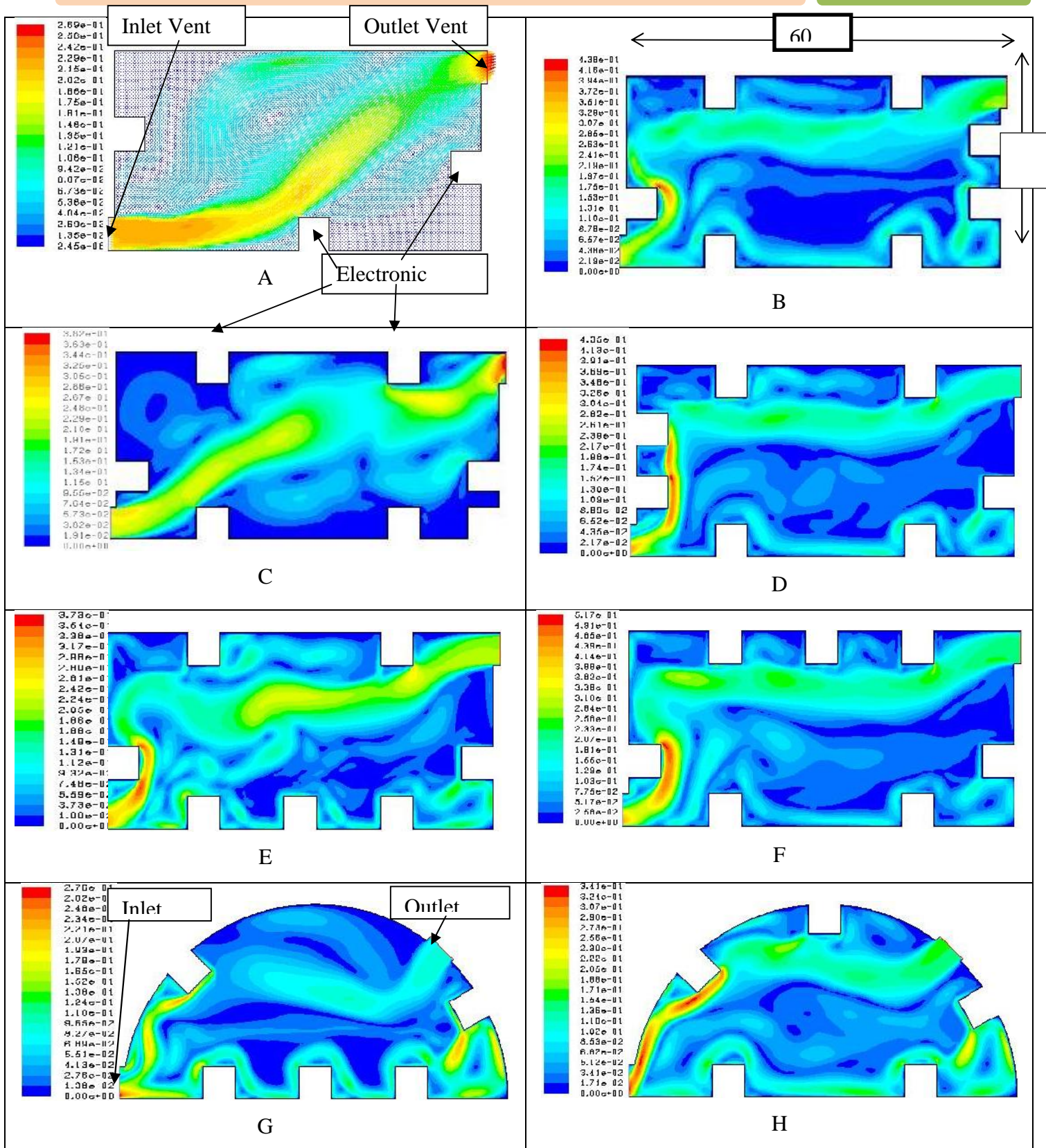


Figure (19). Velocity vectors and contours .

Low temperature-

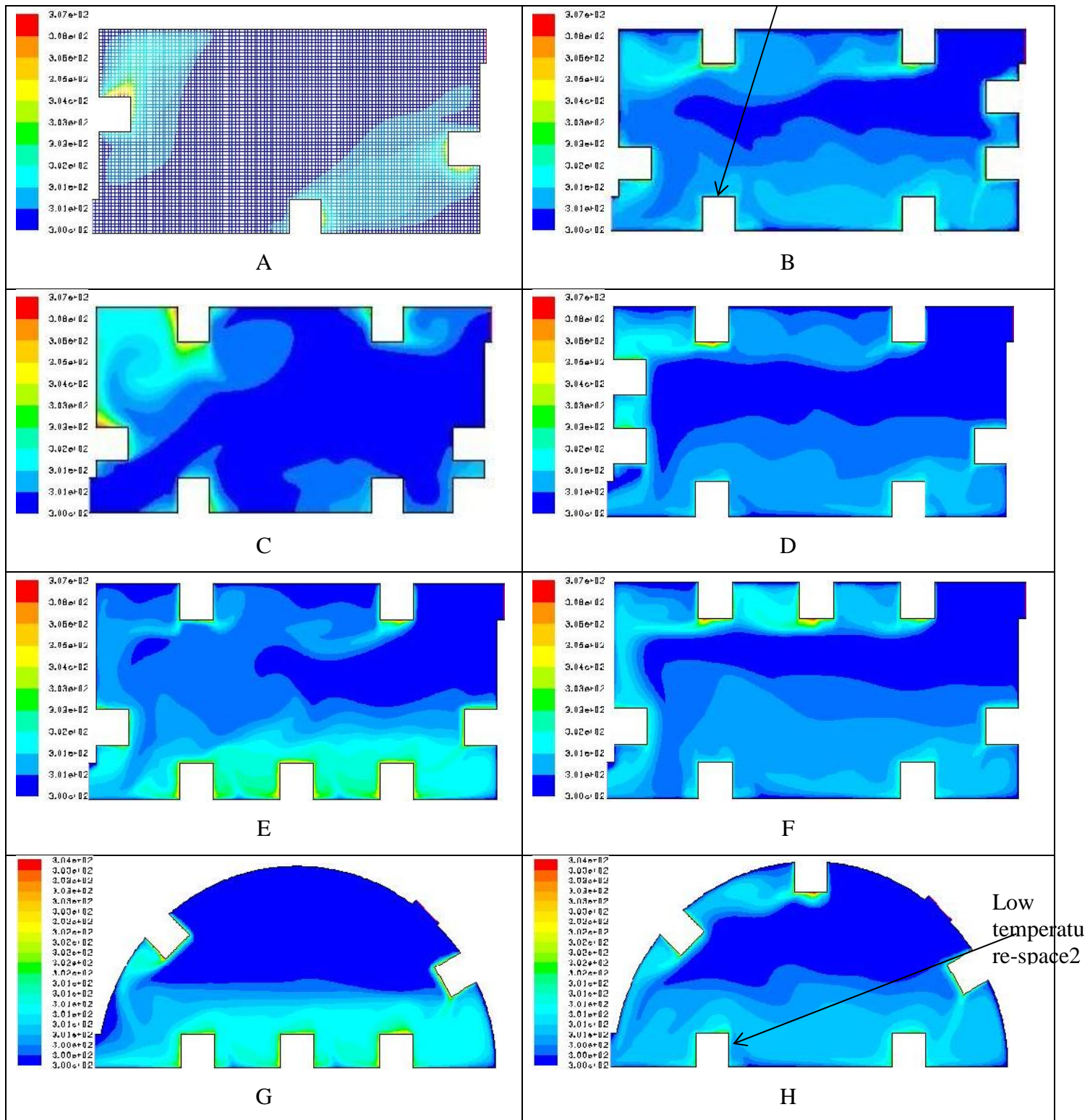


Figure (20). Contours of temperature gradient.

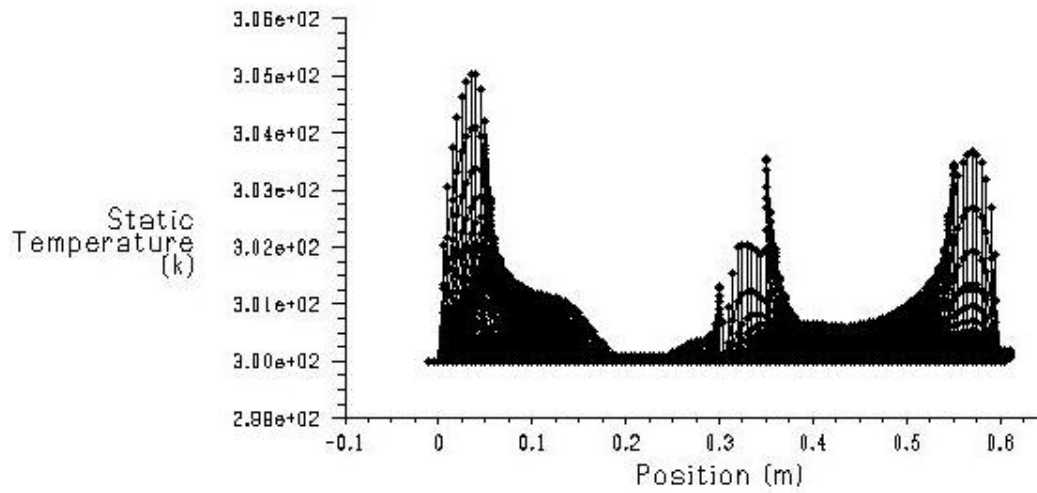


Figure (21). Static temperature with horizontal axis of domain.

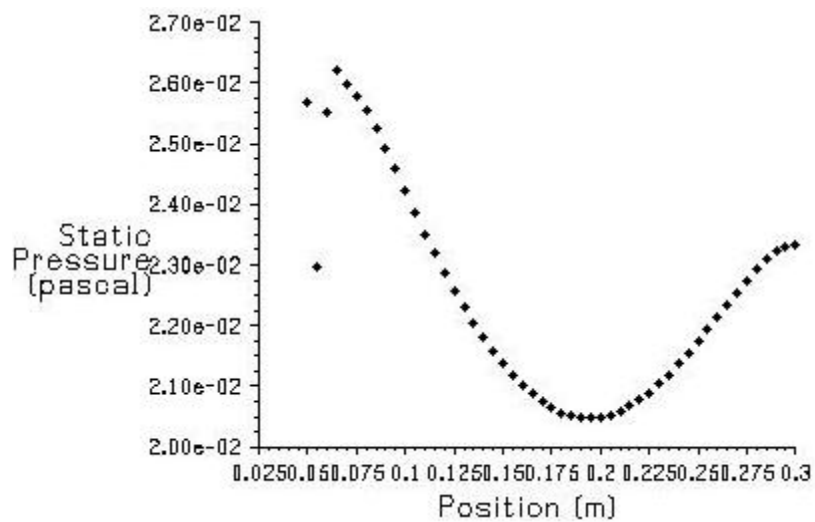


Figure (22). Static pressure curve with position at vertical axis.

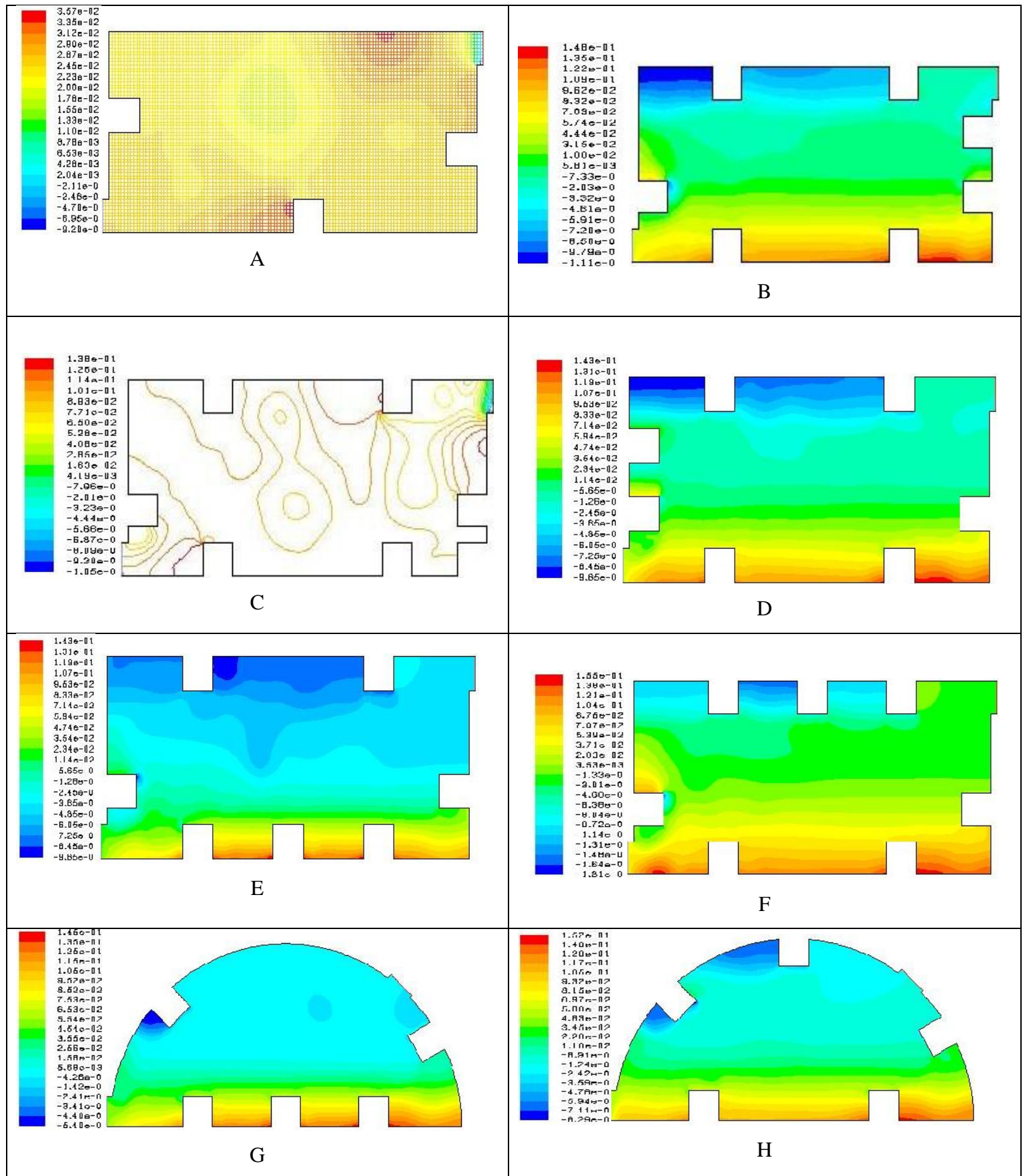


Figure (23) Static pressure contour.

7. Conclusion

The temperature performance of optical receiver consisting of PIN-photodiode and FET-based transimpedance type amplifier is by investigating the effect of various device parameters on receiver performance. The simulation results show that the sensitivity (P_{sen}) of an optical receiver is approximately independent of temperature, of one block, however, as shown in Fig.20, the optimum space for the first block is in space (1), while in the second block the optimum space is (2).

The velocity of air inside the container plays an important role in changing the temperature of chips. So, the chips position has importance in evaluation of heat supply or transferred from one space to another.

The heat generation as a result of electrical power in electronic devices field must be studied to fasten them in proper situation inside the selected block.

8. References

- [1] C. H. Chen and M. J. Deen, "Channel noise modeling of deep submicron MOSFETs," IEEE Trans. Electron Devices, vol. 49, pp. 1484–1487, Aug. 2002.
- [2] H. Shin, J. Jeon and S. Kim, "Analytical Thermal Noise Model of Deep Submicron MOSFETs," Journal of Semiconductors Technology and Science, vol. 6, No. 3, September, 2006.
- [3] B. Claflin, E. R. Heller, and B. Wenningham, "Accurate Channel Temperature Measurement in GaN-based HEMT Devices and its Impact on Accelerated Lifetime Predictive Models," CS MANTECH Conference, May 18th-21st, 2009, Tampa, Florida, USA.
- [4] Claudiu Amza, Ovidiu-George PROFIRESCU, Ioan CIMPIAN, Marcel D. PROFIRESCU, "Monte Carlo Simulation of a HEMT Structures," Proceedings of The Romanian Academy of The Romanian Academy, Volume 9, Number 2, 2008.
- [5] Mustafa Erol, "Effect of Carrier Concentration Dependent Mobility on the Performance of High Electron Mobility Transistors," Turk J Phy, 25 (2001), 137 - 142.
- [6] Wen-Chau Liu, Wen-Lung Chan, Wen-Shiung Lour, Kuo-Hui Yu, Chin-Chuan Cheng, and Shiou-Yinh Cheng, "Temperature-dependence investigation of a high performance

- inverted data-doped V-shaped GaInP/In_xGa_{1-x}As/GaAs pseudomorphic high electron mobility transistor,” IEEE Trans. Electron Devices, vol. 38, no. 7, pp. 1290-1296, 2001.
- [7] Jaluria, Y., “Natural Convection Heat and Mass Transfer”, Pergamon Press, Oxford, 1980.
- [8] Versteeg H.K. and Malalasekera W., “An Introduction to Computational Fluid Dynamics, The Finite Volume Method”, Longman Group Ltd Copyright, England, 1995, (P.41).
- [9] D. C. W. Lo, and S. R. Forrest “Performance of In_{0.53}Ga_{0.47}As and InP junction field effect transistors for optoelectronic integrated circuits. II. Optical receiver Analysis,” Journal of Lightwave Technology, Vol. 7, No. 6, pp. 966-971, June 1989.
- [10] Alok Kushwaha, Manoj Kumar Pandey, Sujata Pandey, and A. K. Gupta, “Analysis of 1/f Noise in Fully Depleted n-channel Double Gate SOI MOSFET,” Journal of Semiconductor Technology and Science, Vol.5, No.3, September, 2005.
- [11] R. S. Fyath, and H. N. Wazeer "Performance Analysis of High Electron-Mobility Transistor for Optical Receiver," M. Sc. Thesis, University of Basrah, College of Engineering, Basrah, Iraq, 2002.
- [12] FLUENT 6.3.26, “User Guide and Manuals”, 2008.
- [13] Ismael M., “Numerical Simulations of Counter Flow Microchannel Heat Exchanger with Different Channels Geometry and Working Fluids”, Ph.D. Thesis, Basrah University, College of Engineering, (2009).
- [14] Gebhart, B., Jaluria, Y., Mahajan, R. L., and Sammakia, B., “Buoyancy Induced Flows and Transport”, Hemisphere Publishing, New York, 1988.

9. Nomenclature

Symbol Definition

x, y	Cartesian coordinates
x_{chip}	horizontal distance of chip
y_{chip}	vertical distance of chip
u, v	velocity component in x, y directions respectively
u_{in}	the velocity input to enclosure
u_{out}	the velocity output from the enclosure

g	gravitational acceleration	
	coefficient of thermal expansion	$\alpha = -\frac{1}{\rho} \left(\frac{\partial \rho}{\partial T} \right)$
μ	Air viscosity	
C_p	specific heat at constant pressure	
k	conductivity	
ρ	density	
\dot{q}	heat generation rate	
p	pressure	
T	temperature	
T_{atm}	atmospheric temperature	
t	time	